ISSN 2278-3091
Volume 12, No.4, July - August 2023
International Journal of Advanced Trends in Computer Science and Engineering
Available Online at http://www.warse.org/IJATCSE/static/pdf/file/ijatcse031242023.pdf
https://doi.org/10.30534/ijatcse/2023/031242023

Satellite Data for Forest Fire Detection using Deep learning

[1]Amir Mokhtar Hannane, [2]Mohamed Anis Benallal
[1,2]Department of computer science, faculty of mathematics and computer science, University of Sciences and Technology of Oran Mohamed Boudiaf (USTO-MB), Oran, Algeria,
[1]amirmokhtar.hannane@univ-usto.dz
[2]mohamed.benallal@univ-usto

Received Date June 14, 2023 Accepted Date: July 25, 2023 Published Date: August 06, 2023

ABSTRACT

Wildfires are devastating natural disasters that cause damage in the earth's ecosystem. Many detection and mapping systems which are created use a lot of tools, including artificial intelligence methods and good human observations. One of the most used systems is satellite. Remote sensing imagery is widely used for forest fire detection (FFD) due to their large zone coverage, which uses traditional and deep learning methods. In the last decade deep learning techniques have given promising results in remote sensing problems. This study uses Landsat-8 images dataset and deep convolutional network method for FFD. The network used in this paper has a special characteristic which is using simultaneously multiple kernels with different sizes. In this work, to improve the performance of forest fire detection, we have used several data in the deep learning input layer: bands 2, 6 and 7 of Landsat-8, and Forest Fire Index value, which is powerful index for FFD. Three different scenarios were used in this study with 3 network configurations for each one, resulting in 9 total distinct models, using multiple kernels of 3x3, 5x5 and 7x7. Landsat-8 images dataset and deep neural network model used in this paper have given good results in detecting forest fires of distinct shapes and different sizes in multiple difficult tests.

Key words: Deep learning, forest fire detection, landsat-8 images, remote sensing data.

1. INTRODUCTION

Forest fires are one of the most devastating natural hazards that cause lots of damages and human losses. In the last few years, it has caused irreversible effects in the world, for example California in 2020 and Australia in 2019. One of the keys to monitor wildfires is to detect and pinpoint exact fire locations, employing artificial computer vision tools, one of the greatest approaches for detecting fire, with optical data or videos from ground, aerial vehicles, and satellite.

Terrestrial and aerial based systems are appropriate tools for fire detection which use optical and infrared cameras, fiber optic sensors or multi sensors for terrestrial systems and unnamed aerial vehicle (UAV) for aerial systems. However, their major inconvenience is the lack of large zone coverage. One of the best alternative options are satellites which cover almost the entire earth. To monitor active wildfires, many satellite sensors were used, for example two imaging sensors created by Earth Observation, MODIS [1] and VIIRS [2].

Wang et al [3] proposed a forest fire monitoring approach based on MODIS data. To evaluate the performance of the proposed technique they used a dataset of MODIS active fire products in china. Experimental results showed that false identification rate was mostly caused by the poor spatial resolution of the MODIS data. To predict the omission error of MODIS fire products, Ying et al [4] made a comparison between fires detected by two approaches. Experiments show that the number of fires detected is much lower as the number of fires in the ground truth map. The day night bands of VIIRS have been used to develop an algorithm for fire nocturnal fire detection [5]. Experimental results suggest that further investigations are needed to improve the process of fire detection. Shukla et al. [6] presented an approach for smoke detection from MODIS dataset images, in which the main purpose was to make distinction between two classes, smoke plumes and clouds. According to the experimental results, the system had the ability at recognizing thick smoke than smoke that was heavily dispersed, but it was still able to extract smokes in the case of other optical data, such as clouds.

Another widely used Earth Observation satellites for FFD are geostationary satellites, Himawari-8, a recent geostationary satellite which is weather satellites operated by the Japan Meteorological Agency that has been used for forest fire monitoring using its sensor called Advanced Himawari Imaging [7] [8]. For example, in the study of Hally et al. [9], a technique for daily temperature fitting of satellite data from the Advanced Himawari Imager is applied. This technique could be divided into two parts. In the first step the Advanced Himawari Imaging bands are aggregated and thereafter in the second step a fitting process is applied in the results of the first

step. Another work using Himawari-8 data is proposed in [10] in which a spatio-temporal fire identification approach is suggested to address the issue of difficulties in tiny fire detection using the brightness temperature.

However, one major inconvenience in mentioned satellites is low spatial resolution, an essential information for accurate forest fire detection and localization. For this problem, a higher spatial resolution satellite sensor should be used, such as Landsat-8, which contains two instruments: Operational Land Imager (OLI) and Thermal Infrared Sensor (TIRS). Recently many algorithms were developed for FFD using remote sensing images, for example Schroeder et al. [11], Murphy et al. [12], and Kumar et al. [13], giving satisfactory results using Landsat-8 spectral bands.

The aim of this study is to present more investigation in using Landsat-8 data for forest fire detection. Furthermore, in this article, we used a deep learning-based method which is a multiple kernel method called "Multiscale-net" with different kernel sizes.

2. FOREST FIRE DETECTION DATASET

Landsat 8 is a U.S. Earth observation satellite launched on February 11, 2013. It consists of the Operational Land Imager instrument and the Thermal Infrared Sensor, both of which are mainly used to measure the temperature of Earth's surface. Landsat 8 has 11 bands; the OLI sensor has 9 bands and TIRS has 2 bands. The table I shows the band number, name, wavelength and resolution for each band [14].

Table 1: Landsat Bands

bands	Band name	Wavelength (μm)	Resolution (m)
Band 1	Coastal Aerosol	0.43 – 0.45	30
Band 2	Blue	0.45 – 0.51	30
Band 3	Green	0.53 – 0.59	30
Band 4	Red	0.64 – 0.67	30
Band 5	Near-Infrared	0.85 – 0.88	30
Band 6	SWIR 1	1.57 – 1.65	30
Band 7	SWIR 2	2.11 – 2.29	30
Band 8	Panchromatic	0.50 – 0.68	15
Band 9	Cirrus	1.36 – 1.38	30
Band 10	TIRS 1	10.6 – 11.19	100
Band 11	TIRS 2	11.5 – 12.51	100

Recently, a new large FFD dataset was published by Almeida et al. [15] (see example in Figure 1). This dataset is created from Landsat-8 images (256x256 pixels) which contain forest fires that are acquired from August to September 2020 in different circumstances [12] and [13].

The corresponding ground truth data set is produced by three studies [13], [11] and [12]. In this study we used only SWIR2, SWIR1, and the blue band. We took a subset of over 28,000 images from 2 continents: Europe and 1/2 of North America in different conditions.

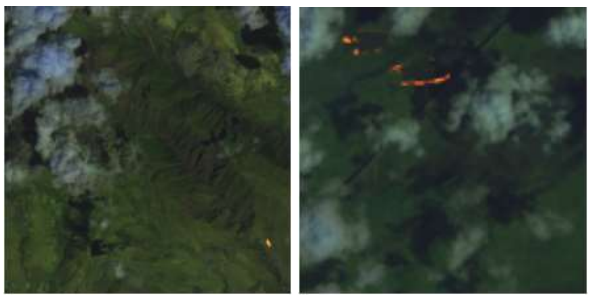

Figure 1: Landsat-8 Dataset Samples

2.1 Forest Fire Index

Thermal and spectral band analysis is the main process of forest fire detection techniques. Previous studies [11] demonstrate that Landsat-8 sensor band 7 (SWIR2) is susceptible to radiation from fire. The Forest Fire Index (FFI), an index for FFD that is derived using SWIR 2, was employed in this study (equation 1).

$$FFI = band\_7\_value / band\_2\_value \quad (1)$$

There are multiple fundamental aspects of FFI may be outlined from equation 1. first, it aids in highlighting the background fire due to its strong reflectance in band 7 and comparatively low reflection in band 2. Second, the removal of smoke, a distracting element in FFD that is frequently seen in the fire zone in satellite data. Smoke appear in the image of band 2, but just marginally in the image of band 7 [16].

3. MULTISCALE-NET DEEP LEARNING MODEL

Multiscale-net architecture is a deep learning encoder/decoder method [17] that uses several kernels and learns an optimal linear or nonlinear combination of kernels within the procedure. This convolution neural network (CNN) is effective for the extraction of spectral and spatial features from remote sensing images. From a bigger pool of kernels, Multiscale-net may choose the best kernel and settings. Additionally, it mixes information from several sources with differing possibilities of similarity, necessitating the use of various kernels.

Multi-kernel learning approaches have been used in many applications, such as hate speech detection [18], high resolution image classification [19] and multimodal neuroimage data fusion [20].

3.1. Network Architecture

To increase the performance of FFD in the used framework, a set of convolutional features with various kernel sizes has been developed. This idea was to use the extracted features on different kernel scales of different sizes to prepare local and general features. Higher levels of features were extracted with deeper convolutional layers, then the maxpooling layer sub-sampled the feature map extracted by the encoder part. On the other hand, the decoder part up-samples the feature maps

by deconvolution layers. Concatenation connections helped the associated decoder get the retrieved features from the encoder.

The encoder part performs five convolution blocks. It uses 3 convolutional layers 3×3, 5×5, 7×7 with 2 padding applied repeatedly. Each convolution follows a batch normalization layer and a rectified linear unit activation function. The number of feature channels is doubled after each convolution block.

Four transposed convolution layers make up the decoder branch, which is a counterpart to the encoder. A 3×3 deconvolution with a stride of 2 precedes each block of the decoder branch, followed by a sequence matching encoder feature maps and two 3×3, 5×5, 7×7 convolutions. Finally, an activation function and a batch normalization layer are applied. Each oversampling procedure results in a decrease of features. In the last layer, a loss function is utilized as a classifier, followed by a 1×1 convolution with an activation

function. Each projected probability is compared to the true class's output, which is 0 or 1.

According on how close the estimated score is to the predicted value, probabilities are determined. This score shows how close or far the predicted values are from the actual value. To reduce this score in the training step, the network framework must be updated with great precision [17].

4. EXPERIMENTAL RESULTS

Four accuracy criteria, were used as quantitative measure of the experimental results: Precision "P", sensitivity "S", F1-Score "F", and intersection on union "I",. The ratio of anticipated to actual firing pixels is known as precision. The proportion of real fire pixels that are successfully recognized is known as sensitivity, or recall. However, because of the probable imbalance between the fire and non-fire classes, the accuracy of the unbalanced dataset may be false, necessitating the calculation of other measures to comprehend the framework's real execution. For this reason, we also used I values, known as the Jaccard Index (JI) [21].

The table 2 shows an abbreviation used for easier and understandable reading, for example: I3K35 means input type I3 with kernels 3x3+5x5.

Table 2: Input Abbreviation of the Model

Input Bands	Input Abbreviation
Blue, SWIR 2, SWIR 1	I3
FFI (SWIR 2/Bleu)	I1
Bleu, SWIR 2, SWIR 1, FFI	I4

The I metric, which measures the proportion of successfully segmented pixels to all ground truth pixels, is the state of the art for semantic segmentation. The evaluation of the statistical accuracy of FFD with 9 configurations using four accuracy criteria: precision, sensitivity, ''I'' and ''F1-Score'' is summarized in Table 3.

1. Input I3: The highest accuracy, sensitivity, F1 score and I are associated with I3K35 (P=86.97%), I3K3 (S=94.74%, F=90.66% and I=82.90%).
2. Input I1: The highest accuracy, sensitivity, F1 score and IoU are associated with I3K35 (P=88.37%, F=87.99%), I3K3 (S=88.12%, I=80.17%).
3. Input I4: The highest accuracy, sensitivity, F1 score and IoU are associated with I3K3 (P=86.27%, S=96.17%, F=90.96% and I=83.41\%).

The Figure 2 represent the outputs of 9 configurations: the first scenario is: input I3, I3K3 output image, I3K35 output images and I3K357 output image. The 2nd scenario is: input I1, I1K3 output image, I1K35 output images and I1K357 output image. The 3nd scenario is: input I4, I4K3 output image, I4K35 output images and I4K357 output image.

Configuration	P	F	S	I
I3K3	86.97%	94.74%	90.66%	90.60%
I3K35	87.50%	91.67%	89.53%	79.16%
I3K357	87.04%	92.22%	89.56%	79.31%
I1K3	86.90%	88.12%	87.50%	80.17%
I1K35	88.37%	87.62%	87.99%	79.44%
I1K357	87.80%	86.79%	87.29%	79.17%
I4K3	86.27%	96.17%	90.95%	83.41%
I4K35	85.30%	90.98%	88.04%	80.51%
I4K357	85.30%	91.32%	88.55%	80.61%

Table 3: Experimental Results By Multiscale-Net Deep Learning Model Using Landsat-8 Dataset.

In the experimental results (see Figure 2) we see that there are slight differences in the image masks and outputs, where most of the fire pixels are detected (same white pixel color in the mask and output), some pixels are detected as fire and are shown as white in the output unlike in the mask which are shown as black pixels (e.g. Figure 2 3rd scenario I4K35) which means that the non-fire area is detected as fire and also means a false alarm. Other pixels are contrary to FP, they are not detected as fire and are shown as black in the output unlike in the mask which are shown as white pixels (e.g. Figure 2, 2nd scenario, I1K35 output image) which means that the fire area is not detected as fire which means FN.

As we can see in the Figure 3 which shows the values of TPs, FPs and FNs in different configurations I3K3, I1K3 and I4K3. The number of TPs and FNs of the scenario I4 was better than the others scenarios. Otherwise, the scenario I1 had the highest FN value. In Figure 3 prove that the use of FFI could improve the process of forest fire detection:

1. I4: More TPs detection and FNs reduction but less reduction in FPs.
2. I1: More FNs reduction but less efficiency in TPs and FPs.

5. CONCLUSION

Forest fires are one of the most damaging hazards to forests and ecosystems. Deep learning approaches have advanced significantly in image/video processing along with technological and artificial intelligence advancements. In this research work, we used the satellites systems for FFD, using Landsat-8 images and a CNN model called "Multiscale-net" which is characterized by the use of convolutional kernels of different sizes simultaneously in each convolutive layer. In total, 9 scenarios were studied and analyzed with 4 accuracy measures based on 3 inputs. I3 corresponds to 3 channel inputs: blue, SWIR2 or SWIR1, I1 corresponds to 1 channel input: SWIR2 / blue (meaning FFI) and I4 corresponds to 4 channel inputs: blue, SWIR2, SWIR1 and (SWIR2 / blue). Each input is tested in three configurations, 3x3 kernel, 3x3+5x5 kernel and 3x3+5x5+7x7 kernel.

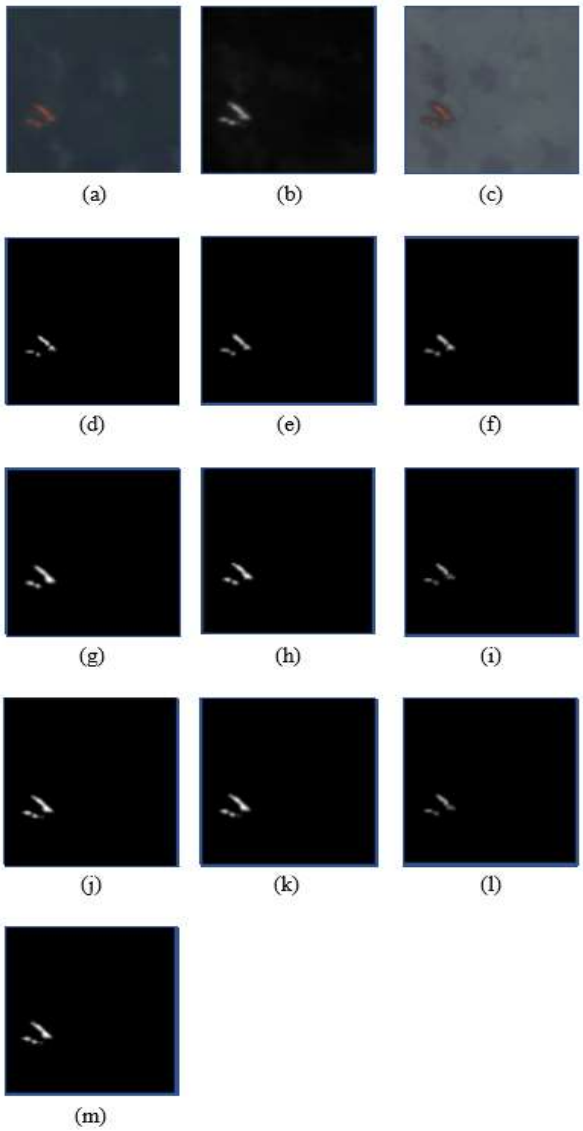

Figure 2: Experimental results. (a) I3 input. (b) I1 input. (c) I4 input. (d) ground truth. (e) I3K3 output. (f) I1K3 output. (g) I4K3 output. (h) I3K35 output. (i) I1K35 output. (j) I4K35 output. (k) I3K357 output. (l) I3K357 output. (m) I4K357 output.

The experimental results were satisfactory, with the highest accuracy being that of the input I1 with the 3x3+5x5 kernels which is 88.37%, and the highest sensitivity, F1-score and I are registered at: 96.17%, 90.95% and 83.41% respectively it belongs to I4 with kernel of 3x3. The addition of FFI plays an important role in reducing FN value and increasing TP and FP values compared to other scenarios.

This study showed the efficiency of landsat-8 imagery, FFI and deep learning method Multiscale-net in forest fire detection. Future studies could be investigated such as using another satellite imagery with higher spatial resolution. Another perspective is to increase the dataset of different regions in the world to generalize a strong forest fire detection model.

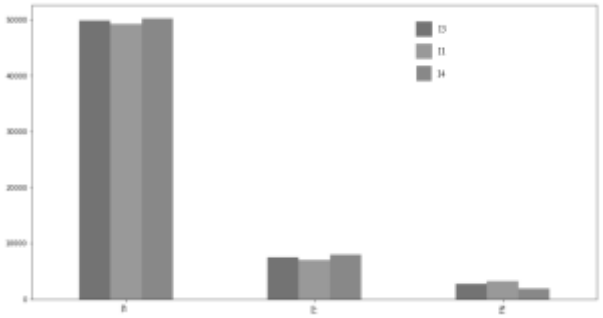

Figure 3: Architecture of the Enhanced Fuzzy Resolution Mechanism using ANFIS

REFERENCES

1. M. Huesca, J. Litago, A. Palacios-Orueta, F. Montes, A. Sebastián-López, P. Escribano, **Assessment of forest fire seasonality using MODIS fire potential: A time series approach**, *Agricultural and Forest Meteorology*, vol. 149, no. 11, pp. 1946–1955, 2009.
2. C. I. Briones-Herrera, D. J. Vega-Nieva, N. A. Monjarás-Vega, J. Briseño-Reyes, P. M. López-Serrano, J. J. Corral-Rivas, E. Alvarado-Celestino, S. Arellano-Pérez, J. G. Álvarez-González, A. D. Ruiz-González, W. M. Jolly, S. A. Parks, **Near Real-Time Automated Early Mapping of the Perimeter of Large Forest Fires from the Aggregation of VIIRS and MODIS Active Fires in Mexico**, *Remote Sensing*, vol. 12, no. 12, p. 2061, 2020.
3. J. Wang, G. Wang, J. Qi, Y. Liu, W. Zhang, **Research of Forest Fire Points Detection Method Based on MODIS Active Fire Product**, *2021 28th International Conference on Geoinformatics*, pp. 1–5, 2021.
4. L. Ying, Z. Shen, M. Yang, S. Piao, **Wildfire Detection Probability of MODIS Fire Products under the Constraint of Environmental Factors: A Study Based on Confirmed Ground Wildfire Records**, *Remote Sensing*, vol. 11, no. 24, p. 3031, 2019.
5. T. N. Polivka, J. Wang, L. T. Ellison, E. J. Hyer, C. M. Ichoku, **Improving Nocturnal Fire Detection With the VIIRS Day–Night Band**, *IEEE Transactions on*

Geoscience and Remote Sensing, vol 54, no. 9, pp. 5503-5519, 2016.

6. B. P. Shukla, P. K. Pal, **Automatic smoke detection using satellite imagery: preparatory to smoke detection from insat-3d**, *International Journal of Remote Sensing*, vol. 30, no. 1, pp. 9–22, 2009.
7. E. Jang, Y. Kang, J. Im, D.-W. Lee, J. Yoon, S.-K. Kim, **Detection and monitoring of forest fires using himawari-8 geostationary satellite data in south korea**, *Remote Sensing*, vol. 11, no. 3, p. 271, 2019.
8. Z. Xie, W. Song, R. Ba, X. Li, L. Xia, **A spatiotemporal contextual model for forest fire detection using himawari-8 satellite data**, *Remote Sensing*, vol. 10, no. 12, p. 1992, 2018.
9. B. Hally, L. Wallace, K. Reinke, S. Jones, A. Skidmore, **Advances in active fire detection using a multi-temporal method for next-generation geostationary satellite data**, *International Journal of Digital Earth*, vol. 12, no. 9, pp. 1030–1045, 2019.
10. C. Zhang, J. Wan, M. Xu, S. Liu, H. Sheng, S, **Spatio-temporal fire detection based on brightness temperature change in Himawari-8 images**, *International Journal of Remote Sensing*, vol. 43, no. 17, pp. 6333–6348, 2022.
11. W. Schroeder, P. Oliva, L. Giglio, B. Quayle, E. Lorenz, F. Morelli, **Active fire detection using landsat-8/OLI data**, *Remote Sensing of Environment*, vol. 185, pp. 210–220, 2016.
12. S. W. Murphy, C. R. de Souza Filho, R. Wright, G. Sabatino, R. Correa Pabon, **HOTMAP: Global hot target detection at moderate spatial resolution**, *Remote Sensing of Environment*, vol. 177, pp. 78–88, 2016.
13. S. S. Kumar, D. P. Roy, **Global operational land imager landsat-8 reflectance-based active fire detection algorithm**, *International Journal of Digital Earth*, vol. 11, no. 2, pp. 154–178, 2018.
14. T. R. Loveland, J. R. Irons, **Landsat 8: The plans, the reality, and the legacy**, *Remote Sensing of Environment*, vol. 185, pp. 1–6, 2016.
15. G. H. de Almeida Pereira, A. M. Fusioka, B. T. Nassu, R. Minetto, **Active fire detection in landsat-8 imagery: A large-scale dataset and a deep-learning study**, *ISPRS Journal of Photogrammetry and Remote Sensing*, vol. 178, pp. 171–186, 2021.
16. M. D. King, S. Platnick, C. C. Moeller, H. E. Revercomb, D. A. Chu, **Remote sensing of smoke, land, and clouds from the NASA ER-2 during SAFARI 2000**, *Journal of Geophysical Research: Atmospheres*, vol. 108, 2003.
17. R. Su, D. Zhang, J. Liu, C. Cheng, **MSU-net: Multi-scale u-net for 2d medical image segmentation**, *Frontiers in Genetics*, vol. 12, p. 639930, 2021.
18. V. Shah, A. Bhole, S. S. Udmale, V. Sambhe, **A Deep Multi kernel Uniform Capsule Approach for Hate Speech Detection**, International Conference on Distributed Computing and Internet Technology: Distributed Computing and Intelligent Technology, pp. 265–271, 2022.
19. W. Liang, Y. Wu, M. Li, Y. Cao, **Adaptive multiple kernel fusion model using spatial-statistical information for high resolution SAR image classification**, *Neurocomputing*, vol. 492, pp. 382–395, 2022.
20. X. Ran, J. Shi, Y. Chen, K. Jiang, **Multimodal neuroimage data fusion based on multikernel learning in personalized medicine**, *Frontiers in Pharmacology*, vol. 13, p. 947657, 2022.
21. L. Hamers, Y. Hemeryck, G. Herweyers, M. Janssen, H. Keters, R. Rousseau, A. Vanhoutte, **Similarity measures in scientometric research: The jaccard index versus salton's cosine formula**, *Information Processing and Management*, vol. 25, no. 3, pp. 315–18, 1989.